RESEARCH ARTICLE

Key Points:
- MMS X-line events cover a wide range of external conditions
- Almost all X-line events are associated with multiple X-lines at the magnetopause
- Reconnection between the magnetosheath and an existing boundary layer is required for KH instability

Correspondence to:
S. A. Fuselier,
sfuselier@swri.edu

Large-scale characteristics of reconnection diffusion regions and associated magnetopause crossings observed by MMS

S. A. Fuselier[1,2] (ID), S. K. Vines[1,2,3] (ID), J. L. Burch[1] (ID), S. M. Petrinec[4] (ID), K. J. Trattner[5] (ID), P. A. Cassak[6] (ID), L.-J. Chen[7,8] (ID), R. E. Ergun[5] (ID), S. Eriksson[5] (ID), B. L. Giles[7] (ID), D. B. Graham[9] (ID), Yu V. Khotyaintsev[9] (ID), B. Lavraud[10,11] (ID), W. S. Lewis[1] (ID), J. Mukherjee[1] (ID), C. Norgren[9] (ID), T.-D. Phan[12] (ID), C. T. Russell[13] (ID), R. J. Strangeway[13] (ID), R. B. Torbert[1,14] (ID), and J. M. Webster[15]

[1]Southwest Research Institute, San Antonio, Texas, USA, [2]Department of Physics and Astronomy, University of Texas at San Antonio, San Antonio, Texas, USA, [3]Now at The Johns Hopkins University Applied Physics Laboratory, Laurel, Maryland, USA, [4]Lockheed Martin Advanced Technology Center, Palo Alto, California, USA, [5]Laboratory for Atmospheric and Space Physics, University of Colorado Boulder, Boulder, Colorado, USA, [6]Department of Physics and Astronomy, West Virginia University, Morgantown, West Virginia, USA, [7]Goddard Space Flight Center, Greenbelt, Maryland, USA, [8]Astronomy Department, University of Maryland, College Park, Maryland, USA, [9]Swedish Institute of Space Physics, Uppsala, Sweden, [10]Institut de Recherche en Astrophysique et Plantologie, Université de Toulouse, Toulouse, France, [11]Centre National de la Recherche Scientifique, Toulouse, France, [12]Space Science Laboratory, University of California, Berkeley, California, USA, [13]Institute for Geophysics and Planetary Physics, University of California, Los Angeles, California, USA, [14]Space Science Center, University of New Hampshire, Durham, New Hampshire, USA, [15]Physics and Astronomy, Rice University, Houston, Texas, USA

Abstract The Magnetospheric Multiscale (MMS) mission was designed to make observations in the very small electron diffusion region (EDR), where magnetic reconnection takes place. From a data set of over 4500 magnetopause crossings obtained in the first phase of the mission, MMS had encounters near or within 12 EDRs. These 12 events and associated magnetopause crossings are considered as a group to determine if they span the widest possible range of external and internal conditions (i.e., in the solar wind and magnetosphere). In addition, observations from MMS are used to determine if there are multiple X-lines present and also to provide information on X-line location relative to the spacecraft. These 12 events represent nearly the widest possible range of conditions at the dayside magnetopause. They occur over a wide range of local times and magnetic shear angles between the magnetosheath and magnetospheric magnetic fields. Most show evidence for multiple reconnection sites.

1. Introduction to Magnetic Reconnection and the Magnetospheric Multiscale Mission

Magnetic reconnection is believed to be a fundamental process that converts magnetic energy into particle energy. This process is universal, occurring at the Sun, in planetary magnetospheres, and in other astrophysical objects like neutron star magnetodisks.

Forty years of observations in the near-Earth plasma environment, combined with theoretical studies and laboratory research, indicate that reconnection is initiated and maintained in a very small region called the electron diffusion region (EDR). The thickness of this central electron diffusion region (in the direction normal to the magnetopause or magnetotail neutral sheet) is approximately one electron skin depth [e.g., *Shay et al.*, 1998; *Mozer et al.*, 2002; *Hesse*, 2006], and the width (in the direction tangential to the magnetopause or the magnetotail neutral sheet) is approximately 10 electron skin depths. At Earth's magnetopause, the EDR dimensions are about 2 km by 20 km (see the recent reviews of magnetic reconnection by *Fuselier and Lewis* [2011] and *Cassak and Fuselier* [2016]). The third dimension, along the magnetopause surface, depends on the length of the reconnection X-line and may be tens of thousands of kilometers long. Inside this small EDR, electrons become demagnetized and the magnetic field lines "break" and "reconnect" across a thin current layer (e.g., across the magnetopause or the magnetotail neutral sheet). Surrounding this region, there is a larger region where electron-scale physics is also evident [e.g., *Mozer et al.*, 2002; *Phan et al.*, 2016]. It is clear from observations, theory, and simulations that understanding reconnection onset, maintenance, and rate requires measuring the electric and magnetic fields and the 3-D electron distributions in and near the inner EDR.

Because the dimensions of the EDR are related to the electron skin depth, the EDRs at the magnetopause and near-Earth magnetotail are the only ones that are large enough and that are close enough to the Earth to be observed in situ by properly instrumented spacecraft. The four-spacecraft Magnetospheric Multiscale (MMS) mission is designed to use Earth's magnetosphere, in particular the magnetopause and near-Earth magnetotail, as a laboratory to study magnetic reconnection [*Burch et al.*, 2016a]. The mission was launched on 12 March 2015 in a 28° equatorial inclination, 12 Earth radii (R_E) apogee elliptical orbit.

The four MMS spacecraft are outfitted with very high time-resolution plasma, electric, and magnetic field instruments, and the spacecraft are placed in orbits that target magnetopause and near-Earth magnetotail EDRs [*Burch et al.*, 2016a; *Fuselier et al.*, 2016a]. The mission is conducted in five phases over 2 years, two phases on the dayside (phases 1a and 1b), two on the nightside (phases 1a and 2b), and one transition phase (phase 2a) from the second dayside to the near-tail nightside phase.

The first phase, phase 1a, focused on magnetopause reconnection and was conducted from 1 September 2015 through 8 March 2016. During this phase, the 12 R_E orbit apogee precessed through the dayside from dusk to dawn. Over 4500 partial and full magnetopause crossings were observed. A partial crossing occurs from the magnetosphere or magnetosheath into the boundary layer or current layer, while a full crossing is from the magnetosphere to the magnetosheath or vice versa. Of these full or partial crossings, there were over 300 where the spacecraft were probably close to the reconnection X-line. In almost all cases, the proximity of the reconnection X-line was confirmed by a switch in the direction of flow of the ion jets in the reconnection exhaust. This switch occurs because the reconnection region passes over the spacecraft [e.g., *Øieroset et al.*, 2001; *Phan et al.*, 2003]. The number of magnetopause crossings near the reconnection X-line is a factor of 10 times higher than the 30 full crossings that were predicted for phase 1a prior to the launch [*Fuselier et al.*, 2016a]. For the predictions, the term "close crossing" was defined as a predicted magnetopause crossing that was within 0.5 R_E (about 3600 km) from the modeled X-line.

Of the 300 crossings close to the reconnection X-line, to date, there are 12 candidate EDR events identified in the phase 1a MMS data set. These reported events occurred either in the "inner" EDR in the immediate vicinity of the X-line or in the surrounding region of the EDR, within one to a few ion skin depths, [e.g., *Phan et al.*, 2007] where electron-scale physics (e.g., nongyrotropic electron distributions, intense current density, and enhanced dissipation) was observed. Here these 12 events are identified as X-line region encounters and called simply "X-line events" to avoid the question whether the encounter was within or near the inner EDR region. The important distinction for these 12 X-line events compared to the 300 crossings close to the reconnection X-line is that in these 12 events, electron-scale physics was observed. A comprehensive search of the data from this phase is not complete; however, based on the small size where electron physics occurs, the small number of events from this first phase of the mission was expected. The small number of events spread over 6 months of observations raises the possibility of observational bias. In particular, the electron physics at and near an X-line may be identified only for a limited range of external parameters, such as interplanetary magnetic field (IMF) orientation and dynamic pressure.

The purpose of this paper is twofold. First, the 12 X-line events are considered as a group to determine if they span the possible range of solar wind and magnetospheric conditions that were encountered during phase 1a. If MMS is investigating a universal, fundamental process, then this investigation should be conducted over the widest range of possible conditions. Conditions that are identified and investigated here include the magnetic shear, the gradient in the plasma beta and the importance of magnetospheric ions, and magnetosheath flow velocities. Second, this paper investigates the larger scale characteristics of the magnetopause crossings that are associated with the X-line events. The MMS mission is focused on revealing the microscale physics of reconnection, and several discoveries have already been made in the X-line region [e.g., *Burch et al.*, 2016b]. However, there are data analysis techniques that provide information on larger scale characteristics. The focus here is on these larger scale characteristics, specifically the location of the X-line and the existence of magnetic islands or multiple X-lines.

Observations in this paper are from the MMS spacecraft field experiment [*Russell et al.*, 2016; *Torbert et al.*, 2016], the Fast Plasma Investigation [*Pollock et al.*, 2016], and the Hot Plasma Composition Analyzer [*Young et al.*, 2016].
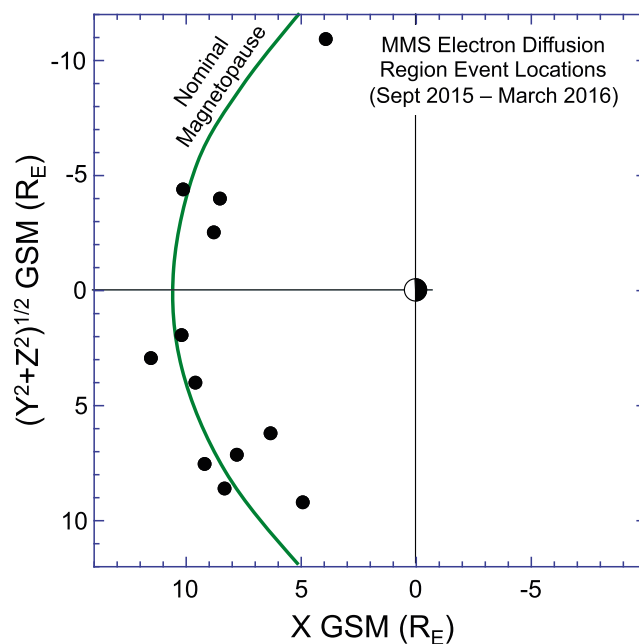
Table 1. Overview Information for the 12 X-Line Region Encounters Observed During Phase 1a From 1 September 2015 to 8 March 2016

Date	X-Line Region Time	Magnetopause Crossing Time	Reference
8 September 2015	11:01:20	11:01:50	*Eriksson et al.* [2016]
19 September 2015	07:43:30	07:41:30	*Chen et al.* [2016]
16 October 2015	10:33:30	10:33:50	*Norgren et al.* [2016] and *Lavraud et al.* [2016]
16 October 2015	13:07:02	13:05:40	*Burch et al.* [2016b]
22 October 2015	06:05:22	06:05:30	*Phan et al.* [2016]
1 November 2015	15:08:06	15:07:05	
12 November 2015	07:19:21	07:19:20	
6 December 2015	23:38:31	23:32:40	*Khotyaintsev et al.* [2016]
8 December 2015	11:20:43	11:20:40	*Burch and Phan* [2016]
14 December 2015	01:17:40	01:17:20	*Graham et al.* [2016]
10 January 2016	09:13:35	09:13:40	
7 February 2016	20:23:35	20:33:40	

2. X-Line Events

Table 1 lists the 12 X-line events from phase 1a that have been identified to date. The date and time of the events are listed in the first two columns. Often, the spacecraft are in the region where electron-scale physics is observed for less than a few seconds as the magnetopause sweeps over the spacecraft (the spacecraft motion is about a factor of 10 slower than the in-and-out motion of the magnetopause). Also listed is the center time in the magnetopause current layer (defined here as a magnetopause crossing) that is close to the X-line event time. The magnetosheath and magnetosphere properties of these magnetopause crossings are investigated in subsequent sections of this paper. Finally, a representative publication of the event (if a publication exists at the time of this writing) is in the last column. These publications focus on the microphysics of a particular event, whereas the focus here is on the larger scale properties of the magnetopause associated with the events as a group.

Figure 1 shows the GSM locations of the events in Table 1 rotated about the X_{GSM} axis into the X, $\pm(Y^2 + Z^2)^{1/2}$ GSM plane. The sign of $(Y^2 + Z^2)^{1/2}$ is determined by the sign of the Y component. The spacecraft encountered the magnetopause south of the $Z_{GSM} = 0$ plane, but the 28° inclination orbit kept the encounters within about 6 R_E of the $Z_{GSM} = 0$ plane. The events are distributed over almost the entire range of local times accessible to the MMS spacecraft in their 12 R_E apogee orbit. Although the number of events is small, there is no indication of a dawn-dusk asymmetry in their occurrence. The locations relative to the nominal position of the magnetopause indicate that the X-line regions were encountered under a wide range of solar wind conditions. All but one of the events occurred under southward IMF conditions. The magnetopause is eroded inward (toward Earth) from its nominal position when the IMF is southward [e.g., *Roelof and Sibeck*, 1993]. However, this erosion is not sufficient to account for magnetopause crossings in Figure 1 that are significantly

Figure 1. Locations of the 12 X-line region events from MMS phase 1a. The events span nearly the entire range of local times accessible to the MMS spacecraft. There is no prenoon or postnoon bias, and the events occur over a wide range of dynamic pressures.

closer to the Earth than the nominal location. Compression of the magnetopause due to higher than nominal solar wind dynamic pressure is also required. Indeed, the solar wind dynamic pressure ranged from 0.9 nPa to 4.6 nPa for the 12 events (with ~1.5 nPa being approximately nominal). A survey of the solar wind dynamic pressure over the entire phase 1a from September 2015 to March 2016 indicates that the dynamic pressures for the 12 events cover 87% of the observed range during mission phase 1a.

3. Magnetic Shear at the Magnetopause

There are two general types of reconnection: antiparallel and component (or guide-field) reconnection (see *Sonnerup* [1974], *Gonzalez and Mozer* [1974], and *Crooker* [1979] and the more recent reviews of *Fuselier and Lewis* [2011], *Paschmann et al.* [2013], and *Cassak and Fuselier* [2016]). At the magnetopause, antiparallel reconnection occurs between magnetosheath and magnetospheric magnetic field lines that are exactly oppositely directed, with a magnetic shear angle across the magnetopause of 180°. For component reconnection, only one component of the magnetosheath and magnetospheric field lines are oppositely directed and the magnetic shear angle across the magnetopause is less than 180°.

Over the past 10 years, an empirical model, called the Maximum Magnetic Shear Model [*Trattner et al.*, 2007a, 2007b], has been reasonably successful in determining where and under what solar wind conditions antiparallel or component reconnection occurs at the magnetopause. This empirical model has been validated independently [*Fuselier et al.*, 2011; *Petrinec et al.*, 2011; *Dunlop et al.*, 2011; *Trattner et al.*, 2012; *Komar et al.*, 2015; *Vines et al.*, 2017; *Trattner et al.*, 2017] and was used in the MMS mission design for the dayside phases 1a and 1b [*Fuselier et al.*, 2016a].

To predict the type of reconnection and its location on the magnetopause, the model requires only the IMF orientation in GSM coordinates. For the observations here, the IMF orientation is determined from the Wind or ACE upstream spacecraft. Although the original model was designed for southward IMF conditions, it is readily extended to northward IMF when the B_z component is dominant. However, when the IMF is northward and B_x or B_y is dominant, the predictions from the Maximum Magnetic Shear Model have not been validated. For the full range of IMF orientations, model predictions fall into six broad categories, three for northward IMF and three for southward IMF. The first category is northward IMF when the $+B_z$ component dominates. The next two categories are northward IMF when either the $\pm B_y$ component or the $\pm B_x$ component dominates. There are three similar categories for southward IMF; when the $\pm B_y$ component dominates, when the $\pm B_x$ component dominates, and when the $-B_z$ component dominates.

Figure 2 shows magnetopause crossings from Table 1 for four X-line events that represent four of the six categories. Each panel shows the shear angles between the model magnetosheath and magnetospheric magnetic fields mapped onto the magnetopause surface and projected onto the Y_{GSM}-Z_{GSM} plane. The view is from the Sun, and the black lines that cut through high shear regions of the magnetopause show the predicted locations of reconnection lines. The black circles show the location of the terminator, and the blue diamonds show the location of the MMS spacecraft.

Clockwise from the top left panel, the 8 September 2015 event occurred under $+B_z$ dominant conditions, the 19 September 2015 event occurred under B_y dominant conditions, the 14 December 2015 event occurred under B_x dominant conditions, and the 12 November 2015 event occurred under $-B_z$ dominant conditions. Thus, the X-line events span the possible range of IMF orientations that determine where and which type of reconnection occurs at the magnetopause with the exception of the combination of $\pm B_y$ dominant or $\pm B_x$ dominant conditions during times of $+B_z$.

In the upper left panel of Figure 2, the reconnection X-lines are at high latitudes, poleward of the magnetospheric cusps and very far away from the low-latitude spacecraft. This 8 September 2015 X-line event occurred during a crossing of the low magnetic shear magnetopause in the presence of Kelvin-Helmholtz (KH) waves. Localized reconnection occurred in the vortex structures of the KH waves [*Eriksson et al.*, 2016; *Vernisse et al.*, 2016], and its location is not predicted by the Maximum Magnetic Shear Model.

The B_y dominant X-line event in the upper right panel was the most common category, representing six other similar events in Table 1 (16 October 2015 (2 events), 22 October 2015, 6 December 2015, 10 January 2016, and 7 February 2016). For B_y dominant conditions, the Maximum Magnetic Shear Model predicts that a
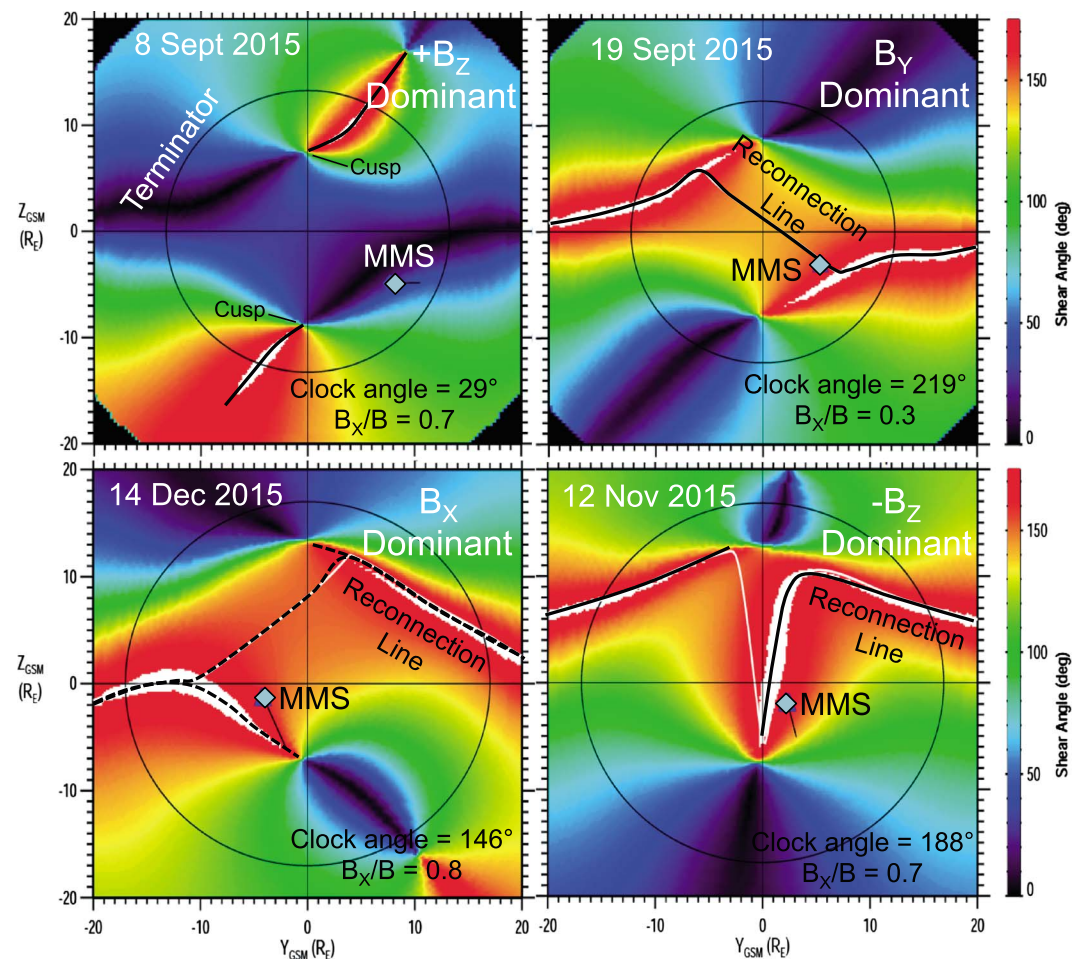
Figure 2. Magnetic shear angles and reconnection X-line locations for four different categories of IMF conditions. The reconnection X-line locations are from the Maximum Magnetic Shear Model. The 12 X-line events fall into these four categories. In the upper left panel, the $+B_z$ dominant conditions occurred for only one event, the 8 September 2015 event. In the upper right-hand panel, the B_y dominant conditions represent the majority of the events (7 out of 12). The B_x dominant and $-B_z$ dominant conditions in the lower left and lower right panels, respectively, represent two events each.

continuous antiparallel and component reconnection line extends across the entire dayside [*Trattner et al.*, 2007a, 2007b]. Antiparallel reconnection occurs on the flanks of the magnetopause, but a component reconnection line (in this case with a minimum magnetic shear of ~140°) links the antiparallel reconnection lines across the dayside. The spacecraft is in an interesting location that is southward and very close to the predicted, component reconnection line but northward of a high magnetic shear region that could contain an antiparallel reconnection X-line. In section 7, evidence is presented that demonstrates that the spacecraft is indeed southward of a component reconnection line.

The B_x dominant X-line event in the lower left panel represents one other event listed in Table 1 (14 December 2015). For B_x dominant conditions, the Maximum Magnetic Shear Model predicts a pair of antiparallel reconnection lines extending from the magnetospheric cusps [*Trattner et al.*, 2007a, 2007b]. The spacecraft are relatively close to the antiparallel reconnection line that originates from the southern cusp. However, the 14 December 2015 event had a strong guide field and was therefore a component reconnection event. The spacecraft are further away from the component reconnection line that links the two antiparallel reconnection lines in the lower left panel of Figure 2. Although not shown, the other event that occurred on 8 December 2015 under B_x dominant conditions was also a component reconnection event [*Burch and Phan*, 2016]. In this case, the spacecraft were relatively close to a component reconnection line. However, the Maximum Magnetic Shear Model predicts only antiparallel reconnection for B_x dominant conditions. Therefore, for these two cases, the predictions from the Maximum Magnetic

Table 2. Densities, Temperatures, and Magnetic Field Strengths for the 12 X-Line Region Encounters Observed During Phase 1a From 1 September 2015 to 8 March 2016

Date	Sheath Time	Density H+ (cm−3)	Density He2+ (cm−3)	Temp. H+ (eV)	B Total (nT)	Sphere Time	Density H+ (cm−3)	Density He2+ (cm−3)	Density He+ (cm−3)	Density O+ (cm−3)	Temp. H+ (eV)	B Total (nT)	Shear Angle (deg)
8 September 2015[a]	11:02:00	19.2	0.62	130	79.5	11:01:10	9	0.32	0.006	0.116	600	69.7	28
19 September 2015	07:41:38	31.7	0.82	400	62.7	07:40:40	3.2	0.021	0.038	0.028	5000	63.6	149
16 October 2015	10:33:40	19.9	0.57	250	22.6	10:32:50	1.04	0.008	0.0004	0.01	4000	39.8	149
16 October 2015	13:06:10	14.0	0.25	300	24.2	13:05:20	1	0.0001	0.0004	0.013	3000	37.9	152
22 October 2015	06:05:40	19.8	0.85	350	26.4	06:04:50	1.1	0	0.062	0.053	2100	57.6	149
1 November 2015	15:01:10	22.4	0.44	210	46.7	15:03:30	4.72	0.12	0.0016	0.038	1300	48.4	168
12 November 2015	07:19:50	8.6	0.17	400	13.3	07:18:40	0.09	0	0	0.007	6000	34.6	165
6 December 2015	23:37:40	17.4	0.66	350	49.9	23:39:00	0.14	0.002	0.002	0.02	3000	65.7	153
8 December 2015	11:20:05	13.0	0.5	550	24.9	11:22:20	0.8	0	0.004	0.024	2100	53.6	129
14 December 2015	01:17:30	7.8	0.45	400	14.5	01:16:50	0.576	0.026	0	0.002	1200	42.9	160
10 January 2016	09:13:20	24.0	0.96	530	35.0	09:16:00	1.2	0.06	0.002	0.01	1700	72.6	144
7 February 2016	20:34:40	16.1	0.6	220	23.9	20:26:50	0.3	0.001	0	0.005	5500	37.3	174

[a]For this event, the plasma and field parameters in the LLBL are substituted for those parameters in the magnetosphere.

Shear Model are not consistent with observations. The shear angle mapping in these two cases should be considered with some caution because, for $|B_x|/|B| > 0.7$, the model magnetosheath magnetic field line draping is not as accurate [*Trattner et al.*, 2007a, 2007b]. Nonetheless, there is clearly an inconsistency with the modeled and observed location of the component reconnection line for B_x dominant conditions. This inconsistency has been observed in other cases [e.g., *Trattner et al.*, 2012] and requires further investigation.

Finally, the $-B_z$ dominant X-line event in the lower right panel also represents one other event in Table 1 (1 November 2015). For $-B_z$ dominant conditions, the Maximum Magnetic Shear Model predicts a pair of antiparallel reconnection lines extending from the magnetospheric cusps [*Trattner et al.*, 2007a, 2007b]. The shape of these antiparallel reconnection lines is highly distorted because of the relatively large value of B_x. In this case, the spacecraft are relatively close to the antiparallel reconnection line (within 1 to 2 R_E) and the magnetic shear angle at the reconnection site was large (see Table 2).

In all X-line events except the 8 September 2015, 22 October 2015, 8 December 2015, and 14 December 2015 events, the spacecraft are within about 1 to 2 R_E of the reconnection line predicted by the Maximum Magnetic Shear Model. Since the model has an uncertainty of approximately the same magnitude, the spacecraft are predicted to be at the X-line within the uncertainty of the model. The 8 September 2015 event is excluded from this comparison with the Maximum Magnetic Shear Model because the model predicts the location of primary reconnection sites and the 8 September event occurs in a localized reconnection X-line associated with KH waves. The 8 December 2015 and 14 December 2015 events occurred when the IMF B_x component was very large ($|B_x|/B > 0.8$), and the 22 October 2015 event occurred when the IMF B_x component was bordering on large ($|B_x|/B = 0.7$). Under these conditions, the model used to determine the draping of the magnetosheath field lines is inaccurate. Therefore, the relatively large distance between the spacecraft and the antiparallel reconnection line (~4 R_E) in Figure 2 (lower left panel) is not considered a failure of the model. Thus, for the applicable parameter range for the other eight X-line events, the Maximum Magnetic Shear Model does a reasonably good job of predicting the location of the X-line in the vicinity of the spacecraft.
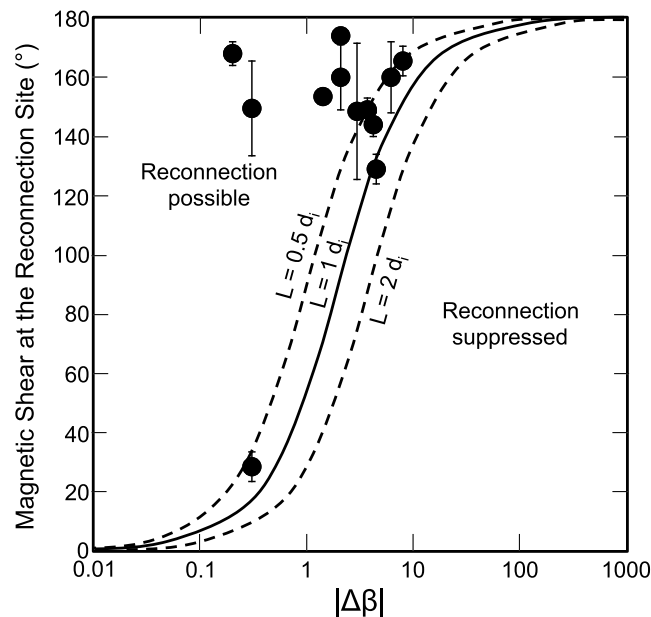
Figure 3. A test of whether the magnetic shear across the magnetopause and change in plasma beta across the magnetopause, $|\Delta\beta|$, for the 12 events are consistent with possible reconnection or suppression of reconnection. All events are consistent with reconnection, even the very low shear event (on 8 September 2015). For this low shear event, the reconnection must be occurring between the magnetosheath and an existing boundary layer.

4. Magnetic Shear, Plasma Beta, and Suppression of Reconnection

Using particle-in-cell simulations of asymmetric reconnection with a guide field, *Swisdak et al.* [2003, 2010] proposed that a density asymmetry across the magnetopause current layer creates a drift of a reconnection X-line. If this density asymmetry is large enough, then the drift speed exceeds the Alfvén speed and reconnection may be suppressed. The condition for suppression depends on the magnetic shear angle, the gradient in plasma beta ($\Delta\beta$) across the magnetopause at the reconnection site, and the thickness of the ion current layer, L_i. This condition has been successfully tested at solar wind current sheets [*Phan et al.*, 2010] at the magnetopauses of Mercury, Earth, and Saturn [*DiBraccio et al.*, 2013; *Phan et al.*, 2013; *Fuselier et al.*, 2014], and even in a laboratory tokamak experiment [*Beidler and Cassak*, 2011]. In previous studies, however, reconnection events were observed far downstream of the X-line, where the locally measured magnetic shear may or may not be representative of the magnetic shear at the X-line [*Phan et al.*, 2013]. Here the data set of X-line events is better suited for testing the theoretical prediction that is based on the conditions across the X-line.

Table 2 contains the data necessary to test this theoretical condition for reconnection suppression for the 12 X-line events in Table 1. The plasma beta in the magnetosheath is computed from the H^+ and He^{2+} densities, the H^+ temperature, and the total magnetic field in the magnetosheath. The plasma beta in the magnetosphere is computed from the H^+, He^{2+}, He^+, and O^+ densities; the H^+ temperature; and the total magnetic field in the magnetosphere. The plasma thermal pressure is computed, assuming that H^+ dominates the pressure in both the magnetosheath and the magnetosphere. This assumption is not valid all the time in the magnetosphere if the heavy ion populations (He^+ and O^+) dominate the plasma mass density. However, in the next section, it is shown that the magnetospheric ions play a relatively minor role in all X-line events in Table 1.

Figure 3 shows the change in plasma beta across the magnetopause, $\Delta\beta$, versus the measured magnetic shear angle at the magnetopause crossing. The measured magnetic shear angle at the crossing is assumed to be the magnetic shear angle at the reconnection site since the crossing is close to an X-line. All of the crossings fall in the $\Delta\beta$ magnetic shear region where reconnection is possible based on *Swisdak et al.* [2010]. Even the crossing where the magnetic shear was only 28° (8 September 2015 event in Tables 1 and 2) had a small enough $\Delta\beta$ for reconnection to be possible. However, for reconnection in the KH vortex structure, $\Delta\beta$ is small enough only if reconnection is occurring between the magnetosheath plasma and an existing boundary layer plasma. If reconnection was occurring between magnetosheath and magnetospheric field lines, then the plasma beta in the magnetosphere is significantly smaller than that in the magnetosheath and $\Delta\beta \approx 1$. Furthermore, the magnetic shear angle from the magnetosheath to the magnetosphere is also smaller, approximately 15°. Thus, the event would be in the "reconnection suppressed" region of the plot.

There are several assumptions in the definition of the curve in Figure 3 that separates possible reconnection from suppression of reconnection [*Cassak and Fuselier*, 2016]. One assumption is that the plasma beta on both sides of the magnetopause is low. Relaxing that assumption results in modification of the change in plasma beta across the magnetopause, where, instead of using the magnetosheath and magnetospheric field strengths to compute the plasma beta in the magnetosheath and magnetosphere, respectively, the average magnetic field strength is used for both terms [see *Cassak and Fuselier*, 2016, equation 6.22]. Although not shown, this modification to $\Delta\beta$ has the effect of shifting all of the points in Figure 3 to the left, or farther into the region of the plot where reconnection is possible. Interestingly enough, this modification does not shift the location of the 8 September 2015 event into the reconnection possible region of the plot when the magnetic shear and (modified) $\Delta\beta$ between the magnetosheath and magnetosphere are considered. Thus, even when the low beta constraint is relaxed, reconnection must be occurring between the magnetosheath plasma and an existing boundary layer plasma for this event. Excluding the 8 September 2015 event, the magnetic shear at the reconnection site for the remaining 11 events is >120°. These events (all under southward IMF conditions) represent a mix of high magnetic shear (>160°), nearly antiparallel events and moderate magnetic shear (between 120° and 160°), component reconnection events. The minimum magnetic shear at the dayside magnetopause for southward IMF is about 90° [*Vines et al.*, 2015]; therefore, these magnetic shear angles span most of the range of possible angles at the dayside magnetopause for southward IMF.

5. Influence of Magnetospheric Ions on the Reconnection Rate

Magnetospheric ions in high concentrations may reduce the reconnection rate at the magnetopause [*Borovsky and Denton*, 2006]. Normally, the magnetosheath plasma density (~20–30 cm^{-3}) is much greater than the ring current plasma density (~0.3 cm^{-3}) in the outer magnetosphere. When reconnection occurs under these conditions, it is highly asymmetric. However, there are two other populations of magnetospheric ions that are much colder and can have significantly higher density than the ring current. These two populations, the warm plasma cloak [*Chappell et al.*, 2008] and the plasmaspheric drainage plume [e.g., *Olsen et al.*, 1987], are both often found at the duskside magnetopause [*Walsh et al.*, 2013; *Wang et al.*, 2015; *Fuselier et al.*, 2016b]. Since their source is Earth's ionosphere, these populations may contain significant concentrations of H$^+$ and heaver ions like He$^+$ and O$^+$.

Using formulations from *Cassak and Shay* [2007] and *Birn et al.* [2008] for the asymmetric, antiparallel reconnection rate, *Borovsky et al.* [2013] developed a formula for the reduction in this rate due to a non-negligible magnetospheric mass density. They used the formula to determine the change in the reconnection rate in global simulations when significant concentrations of magnetospheric ions are present. *Wang et al.* [2015] and *Fuselier et al.* [2016b] determined the reduction in the reconnection rate at the magnetopause for a number of magnetopause crossings in the Cluster and MMS data sets, respectively. They found that the ring current and warm plasma cloak ion populations typically had little effect on antiparallel reconnection at the magnetopause. In a statistical study, *Walsh et al.* [2013] reported a plume at the duskside magnetopause approximately 13% of the time and showed evidence that the reconnection jet velocity was lower for these plume events. They suggested that the plume may slow the efficiency of the reconnection process. However, there has not been a combined survey of both the warm plasma cloak and plasmaspheric plume populations using ion composition to determine if the combined concentrations from both sources and all ion species regularly affect reconnection.

Equation (1) [*Fuselier et al.*, 2016b] is the predicted reduction factor for nonzero magnetospheric mass density to the reconnection rate.

$$R = (1 + \text{MC})^{-\frac{1}{2}}, \tag{1}$$

where (2) defines the mass correction factor, MC.

$$\text{MC} \equiv \rho_M B_{LS} / \rho_S B_{LM} \tag{2}$$

Table 2 contains the mass densities in the magnetosheath and magnetosphere, ρ_S and ρ_M, respectively, and Table 3 contains the L components of the magnetic field in the magnetosheath and magnetosphere, B_{LS} and B_{LM}, respectively. *Fuselier et al.* [2016b] used the total magnetic field in the magnetosheath

Table 3. Predicted Reduction in Reconnection Rate Due To the Presence of Cold Magnetospheric Plasma and Bulk and Alfvén Velocities for the 12 X-Line Region Encounters Observed During Phase 1a From 1 September 2015 to 8 March 2016

Date	Magnetopause Crossing Time	B_{LS} = Magnetosphere Magnetic Field, L Component (nT)	B_{LM} = Magnetosheath Magnetic Field, L Component (nT)	R = Reduction Factor for Reconnection Rate (L Component Only) (No Reduction = 1.00)	V_L = Magnetosheath Bulk Velocity (km/s), L Component	V_{AL} = Magnetosheath Alfvén Velocity (km/s), L Component	V_L/V_{AL}	V_{AL} (Hybrid) = Hybrid Magnetosheath Alfvén Velocity (km/s), L Component	V_L/V_{AL} (Hybrid)
8 September 2015	11:01:50	28	−28	0.90	230	133	1.73	148	1.55
19 September 2015	07:41:30	45	−45	0.95	−230	188	1.22	220	1.04
16 October 2015	10:33:50	40	−32	0.98	−50	148	0.34	216	0.23
16 October 2015	13:05:40	40	−30	0.97	−100	184	0.54	246	0.41
22 October 2015	06:05:30	58	−30	0.98	−50	119	0.42	226	0.22
1 November 2015	15:07:05	38	8	0.98	−45	51	0.88	82	0.55
12 November 2015	07:19:20	10	−12	0.99	−98	107	0.91	115	0.86
6 December 2015	23:32:40	40	−30	0.99	−50	146	0.34	221	0.23
8 December 2015	11:20:40	45	−18	0.98	−150	118	1.27	187	0.80
14 December 2015	01:17:20	32	−20	0.98	−75	156	0.48	222	0.34
10 January 2016	09:13:40	66	−40	0.98	−160	165	0.97	264	0.61

and magnetosphere in equation (2). However, here B_{LS} and B_{LM} are the L components of the magnetosheath and magnetosphere, respectively. The L components from the LMN boundary normal coordinate system are used here because they represent the part of the total magnetic field that is reconnecting. In the LMN coordinate system, the L component is tangential to the magnetopause and has the largest change across the boundary; the M component is perpendicular to L, tangential to the magnetopause, and generally has intermediate change; and the N component is normal to the boundary. The L component magnitude is not very sensitive to the choice of the normal direction and, where within the time sequence of a crossing the magnetic field is measured, with uncertainties of 10–20% of the values listed in Table 2.

Table 3 also shows the results from applying equation (1) to the 12 X-line events. For most of the events, the reduction in the reconnection rate was less than 2%. The 8 September 2015 event had the highest reduction in the reconnection rate (10%). However, the reason for this relatively high reduction was that the reconnection occurred between the magnetosheath and an existing boundary layer. In that reconnecting boundary layer, the O^+ density was the highest for all the events, but H^+ (of magnetosheath origin) still dominated the plasma mass density. Thus, the magnetospheric plasma was not the major cause of the reduction in the reconnection rate.

The 19 September 2015 and the 1 November 2015 events demonstrate the importance of the magnetic field in equation (2) as a mitigating factor in the reduction of the reconnection rate due to the mass density asymmetry at the magnetopause. The ratio of the magnetosheath and magnetosphere mass densities is approximately 10 for the 19 September 2015 event and approximately 4 for

the 1 November 2015 event. However, the predicted reductions in the reconnection rate are 5% for the 19 September 2015 event and only 2% for the 1 November 2015 event because the L component of the magnetosheath magnetic field is the same as that in the magnetosphere for the 19 September 2015 event. It is also significantly smaller than that in the magnetosphere for the 1 November 2015 event. Typically, the magnetic field in the magnetosheath is about a factor of 2 smaller than that in the magnetosphere. This difference in field strengths helps mitigate the influence of magnetospheric ions on the reconnection rate.

Excluding the 8 September 2015 event and considering the remaining events as a group, Table 3 shows that the magnetospheric ion populations have a relatively small predicted effect on reconnection and reconnection for these events is therefore highly asymmetric. It remains to be seen from surveys of all of the magnetospheric ion populations whether this result is typical of the dayside magnetopause reconnection regions.

6. Magnetosheath Flow Velocities

Reconnection may proceed in the presence of a flow shear at the magnetopause, provided that the flow shear is not too large. How large the flow shear can be before a reconnection X-line must move has been the subject of theoretical and observational studies. *Cowley and Owen* [1989] suggested that the reconnection site is stationary if the magnetosheath flow is sub-Alfvénic. If the magnetosheath flow is between 1 and 2 times the Alfvén speed, then reconnection X-lines may convect with the magnetosheath flow such that the flow is Alfvénic in the deHoffmann-Teller frame [see, e.g., *Gosling et al.*, 1991], but reconnection is not possible if the magnetosheath flow is faster. Observations at the high-latitude magnetopause [*Fuselier et al.*, 2000; *Lavraud et al.*, 2005a] and on the flanks [*Gomez et al.*, 2016] of stable reconnection X-lines in magnetosheath flow conditions that were marginally sub-Alfvénic appear to support this suggestion. However, there is also evidence of motion of the X-line in the presence of magnetosheath flow [*Wilder et al.*, 2014] and a suggestion that an isolated reconnection X-line may convect with the flow even if the flow is sub-Alfvénic [*Doss et al.*, 2015]. Finally, with the exception of the *Doss et al.* [2015] study, the question of which Alfvén velocity should be used when determining whether the bulk flow velocity is super-Alfvénic or sub-Alfvénic has not been addressed. For asymmetric reconnection, a hybrid Alfvén velocity is derived from the conservation of mass, energy, and magnetic flux across the magnetopause [*Cassak and Shay*, 2007]. The hybrid Alfvén velocity is

$$V'_{AL} \sim (B_{LM}B_{LS}/2\mu_0)(B_{LM} + B_{LS})/(\rho_M B_{LS} + \rho_S B_{LM})$$ (3)

where the quantities in equation (3) are the same as those defined for equation (2). This hybrid velocity has been used to compare with the reconnection flow jets at the magnetopause [e.g., *Walsh et al.*, 2013]. However, there is no theoretical work that suggests this is the appropriate speed to consider. In fact, *Doss et al.* [2015] suggested that for asymmetric reconnection at an isolated X-line, the relevant speed to consider is the hybrid Alfvén velocity times a large multiplicative factor. In their study, the reconnection X-line always convected with the component of the bulk flow perpendicular to the line at almost any multiple of the Alfvén velocity as computed with the reconnecting, or L component of the magnetic field.

The last five columns of Table 3 show the L component of the magnetosheath bulk velocity, the L component of the magnetosheath Alfvén velocity, the ratio of these two velocities, the hybrid Alfvén velocity (computed using equation (3) with the density parameters in Table 2 and magnetic field L components in Table 3), and the ratio of the L component of the bulk velocity and the L component of the hybrid Alfvén velocity.

For most X-line events, $V_L/V_{AL} < 1$ and, according to *Cowley and Owen* [1989], the reconnection X-line should be stationary for these events. The low values of the ratio are not surprising because the 12 R_E apogee of MMS during phase 1a limits magnetopause crossings between about 07:00 and 16:00 local time (LT). Significant flow velocities in the magnetosheath typically do not occur until past the terminator (i.e., at less than 06:00 LT or greater than 18:00 LT). Three of the 12 X-line events have $V_L/V_{AL} > 1$, but none have a ratio greater than 2. According to *Cowley and Owen* [1989], the three events (8 September 2015, 19 September 2015, and 8 December 2015) should convect in the L direction with the magnetosheath flow. The last column in Table 3 shows that using the L component of the hybrid Alfvén velocity, only one event (8 September 2015) has V_L/V_{AL} (hybrid) substantially greater than 1. Within the ~10–20% uncertainties in this ratio, it is likely that this is the only super-Alfvénic flow event listed in Table 1. Observations discussed in section 7 (below)

from 19 September 2015 are interpreted as evidence of a stationary X-line for this event, in agreement with the possible sub-Alfvénic flow (at least using the hybrid Alfvén velocity).

7. Stability of Reconnection X-Lines and Magnetic Islands

Two-dimensional simulations of reconnection show the development of multiple X-lines with magnetic islands in between them [e.g., *Drake et al.*, 2006a, 2006b]. Magnetic islands have been observed at the magnetopause and, at least in one instance, their scale size was estimated from in situ observations to be of the order of 100 to 250 km [*Teh et al.*, 2010]. Larger and more complex islands also have been observed at the magnetopause. In three dimensions, these larger islands are magnetic flux ropes flanked by active X-lines [e.g., *Hasegawa et al.*, 2010; *Øieroset et al.*, 2011, 2014, 2016]. For one event in the MMS data set, the island structure and separation between the two X-lines was estimated to be approximately 8000 km [*Øieroset et al.*, 2016]. Observations at the magnetopause and in the magnetospheric cusps have been used to argue for even larger island structures of many tens of thousands of kilometers [*Fuselier et al.*, 2011; *Trattner et al.*, 2012]. However, precipitation signatures in the cusp that might be associated with very large island structures are rare, suggesting that these scale sizes are not common [*Trattner et al.*, 2012]. Finally, a recent survey of magnetic islands at the magnetopause concluded that they are present at some scale size for more than 80% of the magnetopause crossings that were relatively near (within a few Earth radii of) a reconnection X-line [*Vines et al.*, 2017]. Thus, magnetic islands are expected to be common for the MMS X-line events.

A variety of observational features have been used to identify magnetic islands at the magnetopause. Electron observations in the reconnection exhaust on the magnetosheath side of the magnetopause provide a very reliable means for determining the topology of magnetic field lines and identifying magnetic islands and multiple reconnection sites. These suprathermal electrons are good tracers of topology because they carry the heat flux, while lower energy electrons are less mobile because they maintain quasi-neutrality. In particular, the observation of either unidirectional or bidirectional streaming of heated electrons in the magnetosheath boundary layer (MSBL) on the magnetosheath side of the magnetopause indicates whether there are one or two active X-lines at the boundary. The MSBL is defined as the reconnection exhaust region on the magnetosheath side of the magnetopause current layer between the separatrix (or separatrices) and the $B_L = 0$ crossing of the current layer. This region could be on open field lines in the exhaust of a single X-line or on closed field lines in the exhausts of two X-lines.

Unidirectional and bidirectional streaming electron signatures have been used to determine the topology of reconnected magnetic field lines when the IMF is northward [*Fuselier et al.*, 1995; *Øieroset et al.*, 2001; *Lavraud et al.*, 2005b, 2006; *Fuselier et al.*, 2012] and when the IMF is southward [*Hasegawa et al.*, 2010; *Fuselier et al.*, 2011; *Øieroset et al.*, 2015] and were used in the recent survey of magnetic islands at the magnetopause [*Vines et al.*, 2017]. These streaming electron signatures observed by a spacecraft crossing the magnetopause in the vicinity of a single X-line and in between multiple X-lines are shown schematically in Figure 4. The left-hand panels show the magnetic field and electron fluxes parallel and antiparallel to the magnetic field as a function of time for three different crossing scenarios, and the right-hand panel shows a schematic of the two-dimensional field structure for two active X-lines at the magnetopause. The parallel and antiparallel fluxes are shown for an energy that is well above the ~100 eV nominal magnetosheath energy. At the magnetopause, magnetosheath electrons are heated to several times this nominal energy [e.g., *Gosling et al.*, 1990; *Fuselier et al.*, 1995]. These electrons stream out of the magnetosphere with broad pitch angle extent, extending to 90° pitch angles [*Fuselier et al.*, 1995; *Vines et al.*, 2017]. There is also a population of higher energy magnetospheric electrons, at energies of tens of keV, that leak out of the magnetosphere along open field lines. This population is distinguished from the magnetosheath electrons heated at or near the magnetopause by its higher energy.

For crossing A in Figure 4, the top left-hand panel shows these signatures for a spacecraft that traverses the magnetopause from the magnetosphere to the magnetosheath on a trajectory that is above (or poleward of) a single X-line. The dayside low-latitude boundary layer (LLBL) is defined here as the reconnection exhaust region on the magnetospheric side of the magnetopause current layer between the separatrix (or separatrices) and the $B_L = 0$ crossing of the current layer. Like the MSBL, the LLBL could be on open field lines in the exhaust of a single X-line or closed field lines in the exhausts of two X-lines. In the LLBL for crossing A in Figure 4, B_z is positive and the electron fluxes parallel and antiparallel to the magnetic field are relatively high.
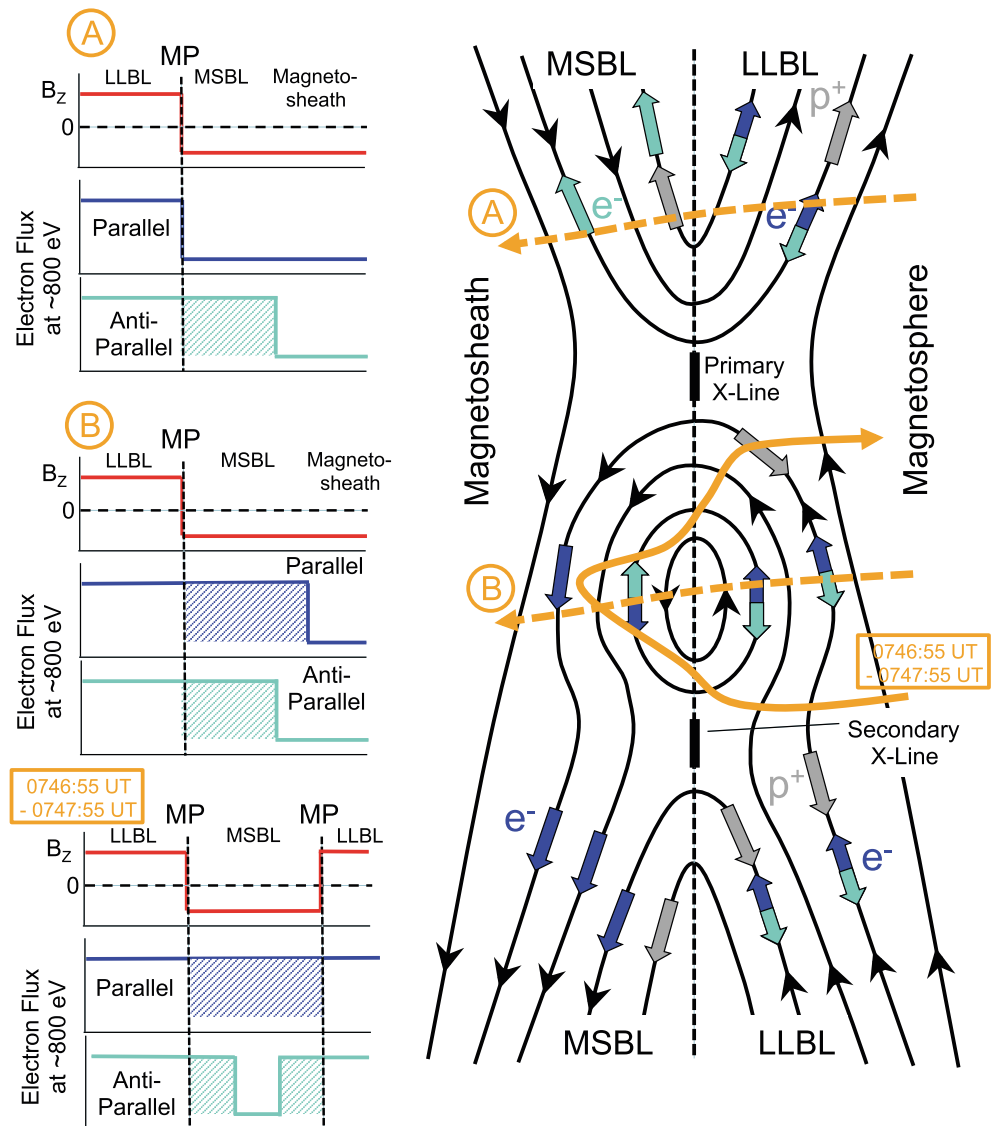
Figure 4. Time variations of heated, streaming electron fluxes parallel and antiparallel to the magnetic field in the MSBL for a magnetopause with a primary and secondary X-lines and a magnetic island between the two X-lines. A spacecraft traversing the magnetopause on trajectory A would observe heated, streaming electrons propagating antiparallel to the magnetic field in the MSBL. A spacecraft on trajectory B would observe heated, streaming electrons both parallel and antiparallel to the magnetic field at first, and then later observe the electrons parallel to the magnetic field. The electron signatures in Figure 5 from 07:46:55 to 07:47:55 UT on 19 September 2015 are consistent with the third trajectory.

Heated electrons produced at the magnetopause propagate parallel to the field lines in the LLBL to the ionosphere, where they mirror and return to the lower latitude reconnection site in the LLBL. The propagation time is of the order of seconds; therefore, there is little to no difference between the parallel and antiparallel fluxes as long as the spacecraft is relatively far from the reconnection site. When the spacecraft is close to the reconnection site, as is the case here, there could be timing differences between the parallel and antiparallel fluxes. In either case, it is difficult to use the electron observations in the LLBL to determine magnetic topology. Upon crossing the magnetopause and entering the MSBL, B_z becomes negative and the parallel electron flux decreases to its value in the magnetosheath "proper," where the spacecraft is not magnetically connected to a reconnection site. The antiparallel electron flux is still high as heated electrons from the magnetopause stream out into the MSBL on open field lines. The streaming direction in the MSBL identifies the direction of the single X-line with respect to the spacecraft location at the magnetopause. In crossing A, the spacecraft traverses the magnetopause above or northward of the

reconnection X-line. For a crossing below, or southward of a single reconnection X-line, the heated electrons would stream parallel to the reconnected field lines into the MSBL.

For crossing B, the spacecraft crosses an island (or flux rope in three dimensions). In the LLBL, the electron signatures are the same as for crossing A. Qualitatively, the electron signatures in the MSBL are similar to crossing A, with one important difference. After crossing the magnetopause and entering the MSBL, heated electrons are observed both parallel and antiparallel to the magnetic field. Later, the antiparallel flux decreases and heated electrons stream parallel to the field only (because the primary reconnection X-line is above the spacecraft). Thus, the unambiguous signature of a magnetopause crossing between two active X-lines is the bidirectional streaming, heated electrons in the MSBL.

While the streaming electrons in the MSBL provide unambiguous evidence of one or two active X-lines, they do not provide information on the distance to the X-line or lines or the two-dimensional size of the magnetic islands or flux ropes. Multispacecraft observations at the magnetopause do provide information on the distance to an X-line, the extent of the X-line, and the size of magnetic islands; however, this information is limited because the MMS spacecraft are very close together (e.g., there are 40 km spacecraft separations for the 19 September 2015 event). As pointed out at the beginning of this section, magnetic islands may have a range of sizes from hundreds of km to tens of thousands of km. The ~10–50 km separations of the MMS spacecraft in mission phase 1a are not sufficient to distinguish among scale sizes greater than 100 km.

Figure 5 shows observations from MMS4 from the 19 September 2015 magnetopause crossing. The panels from top to bottom are the energy-time spectrogram of the H^+ omnidirectional flux from Hot Plasma Composition Analyzer, the B_z GSM magnetic field component, the electron energy-time spectrogram of the electron flux from the Fast Plasma Investigation Dual Electron Spectrometer (FPI-DES), and the parallel and antiparallel electron fluxes at 800 eV from FPI-DES. Five minutes of data are shown with slightly over 4 min of burst mode data from 07:46 UT to about 07:50 UT (with 30 ms FPI-DES distributions) and 1 min of fast survey mode data from 07:50 to 07:51 UT (with 4 s FPI-DES distributions).

The spacecraft starts in the magnetosphere and LLBL. There is a full crossing of the magnetopause from 07:46:50 to 07:46:58 UT, and after a short interval in the MSBL, the spacecraft returns to the current layer. It spends several minutes in this layer before returning to the MSBL at 07:49:08 UT and, finally, into the magnetosheath at the very end of the time interval. There are two time intervals in the MSBL from 07:47 UT to 07:47:30 UT and from 07:49:08 UT to 07:51 UT where the electron fluxes at 800 eV parallel and antiparallel to the magnetic field provide information on the number of active X-lines and the location of the spacecraft relative to these X-lines.

In the first interval, the spacecraft crosses the magnetopause current layer and enters a region where the parallel and antiparallel fluxes are high and nearly equal. About 10 s later (at the dashed line at 07:47:08 UT), the spacecraft enters a region in the MSBL where the parallel flux is higher than the antiparallel flux. The spacecraft transitions out of this region at the dashed line at 07:47:22 UT and returns to a region where the parallel and antiparallel fluxes are nearly equal. Starting at about 07:47:30 UT, the B_z component of the magnetic field begins to rotate as the spacecraft crosses the magnetopause current layer eventually back into the magnetosphere for a short time centered at about 07:47:55 UT. The brief return to the magnetosphere is marked by the low-energy (~10 eV) H^+ fluxes in the top panel.

The two periods of bidirectional streaming electrons in the MSBL indicate that the spacecraft was between two active X-lines. The interval of unidirectional, parallel streaming electrons centered at about 07:47:25 UT indicates that the spacecraft was southward of a single X-line. The magnetic topology of the MSBL interval between the magnetopause crossings at 07:46:55 UT and 07:47:55 UT is shown schematically in the bottom left-hand and right-hand panels of Figure 4. The spacecraft crosses the magnetopause and enters a magnetic island between two active X-lines where there are heated, streaming electrons in both directions along the magnetic field. The magnetopause moves further away, and the spacecraft transitions onto open magnetic field lines that are connected to a single, "primary" X-line that is northward of the spacecraft. Finally, the spacecraft crosses back into the magnetosphere through the magnetic island.

The electron signatures in the second interval from 07:49:08 UT to 07:51 UT are more complicated than those in the first interval, but the two MSBL intervals have several similar characteristics. Starting at 07:49:10 UT, there are two bursts of heated electrons streaming parallel to the field. These bursts indicate that the
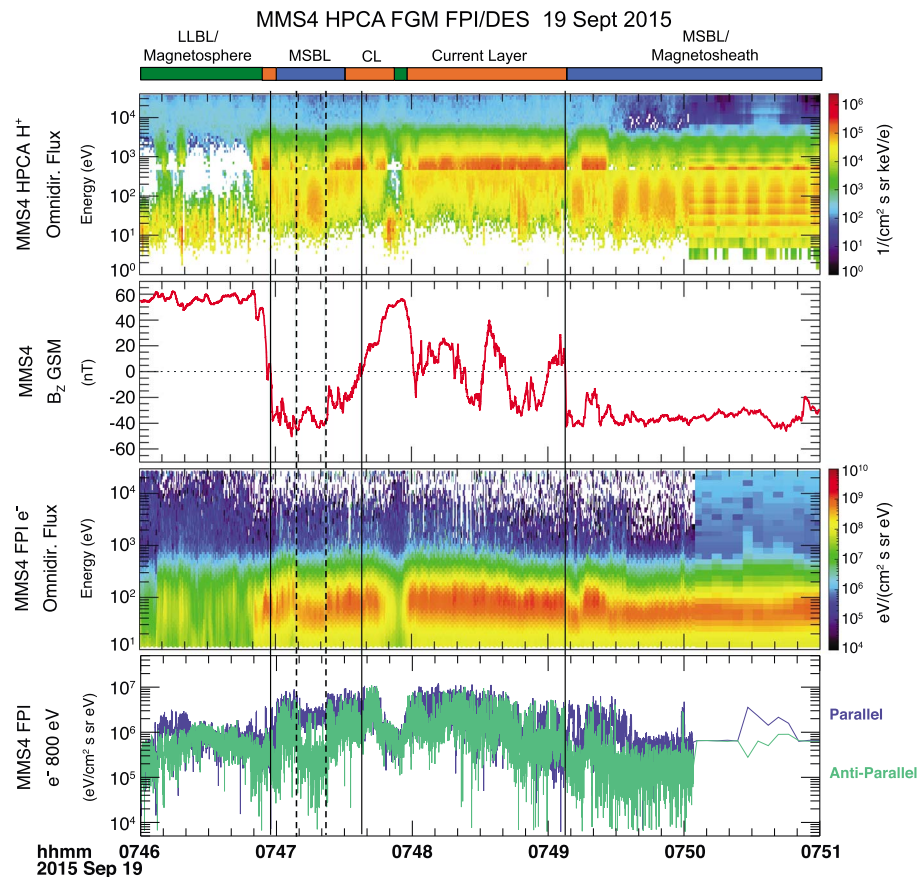
Figure 5. Observations from the magnetopause crossing associated with the event on 19 September 2015. (top to bottom) The proton omnidirectional flux, the B_z component of the magnetic field, the electron omnidirectional flux, and the 800 eV electron flux parallel and antiparallel to the magnetic field. In two MSBL intervals, the spacecraft observes bidirectional, enhanced 800 eV electron fluxes and unidirectional, enhanced 800 eV fluxes parallel to the magnetic field. The nesting of these enhanced electron fluxes from 07:46:55 UT to 07:47:55 UT is consistent with the spacecraft traversing an island structure between two reconnection lines as shown in the right-hand side of Figure 4. The second MSBL interval starting at 07:49:10 UT is not only more complex but also consistent with a magnetic island between two X-lines.

spacecraft was southward of a single X-line, similar to the first interval at 07:47:25 UT. These bursts are followed by several intervals where there are bidirectional streaming electrons and another interval where there are unidirectional heated electrons that are streaming parallel to the field. These intervals indicate transitions into the island structure between two active X-lines and then transition onto field lines connected to the single X-line. Finally, at 07:49:35 UT, the spacecraft crosses the separatrix and is on magnetosheath field lines that are not connected to any reconnection X-line. On these field lines, there are no heated, streaming electrons in either direction along the field. There is a brief transition back onto reconnected field lines at 07:50 UT and then a longer transition back onto reconnected field lines at 07:50:30 UT. Throughout these intervals in the MSBL, MMS4 never observes heated electrons streaming antiparallel only. Thus, the spacecraft is never northward of the primary reconnection X-line in Figure 4 or equivalently, the reconnection line never convects southward to cross the spacecraft. These observations are consistent with the prediction in the top, right-hand panel of Figure 2 that the MMS spacecraft were southward of a component reconnection line. Apparently, this reconnection line remains northward of the spacecraft over the several minutes of the magnetopause crossing in Figure 5.

The interpretation of the magnetic field structures in the magnetopause crossing in Figure 5 assumes a quasi-steady structure that moves slightly northward/southward and inward/outward at a speed much faster than the spacecraft motion. There is certainly a time dependence in the reconnection process because magne-tosheath and magnetospheric field lines reconnect first at the primary X-line in Figure 3 and then at the
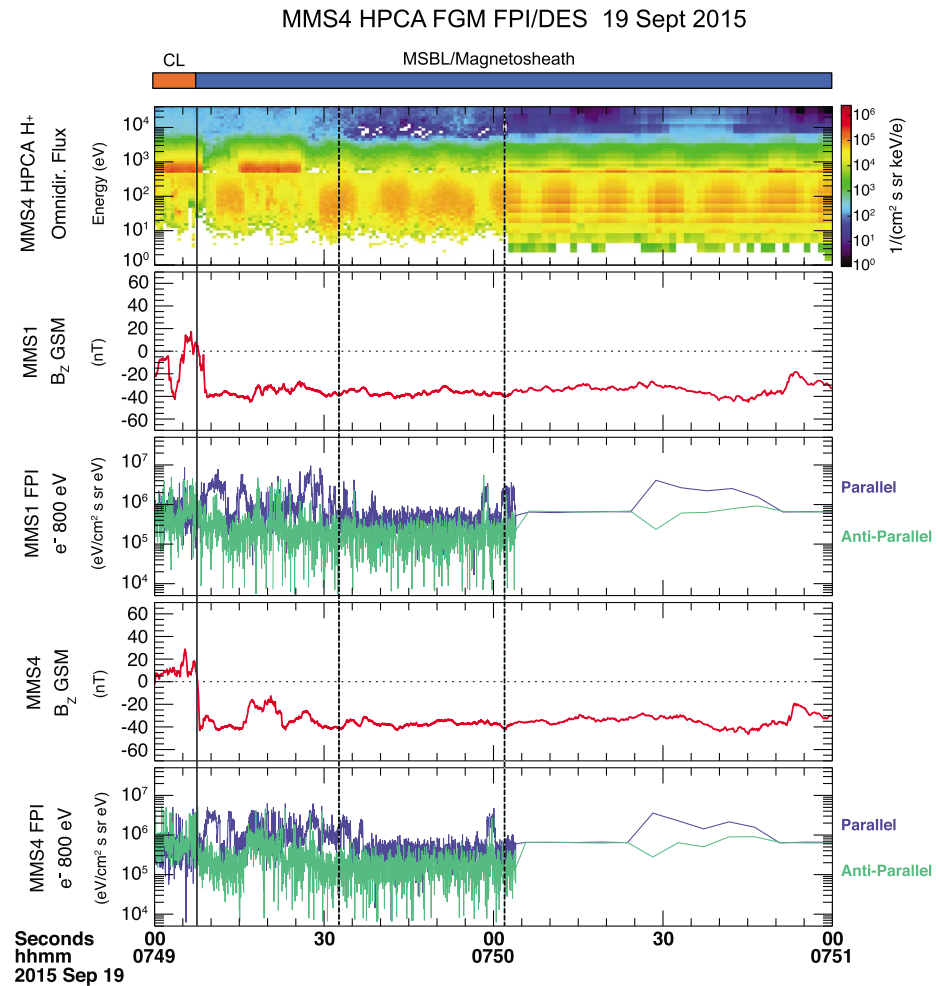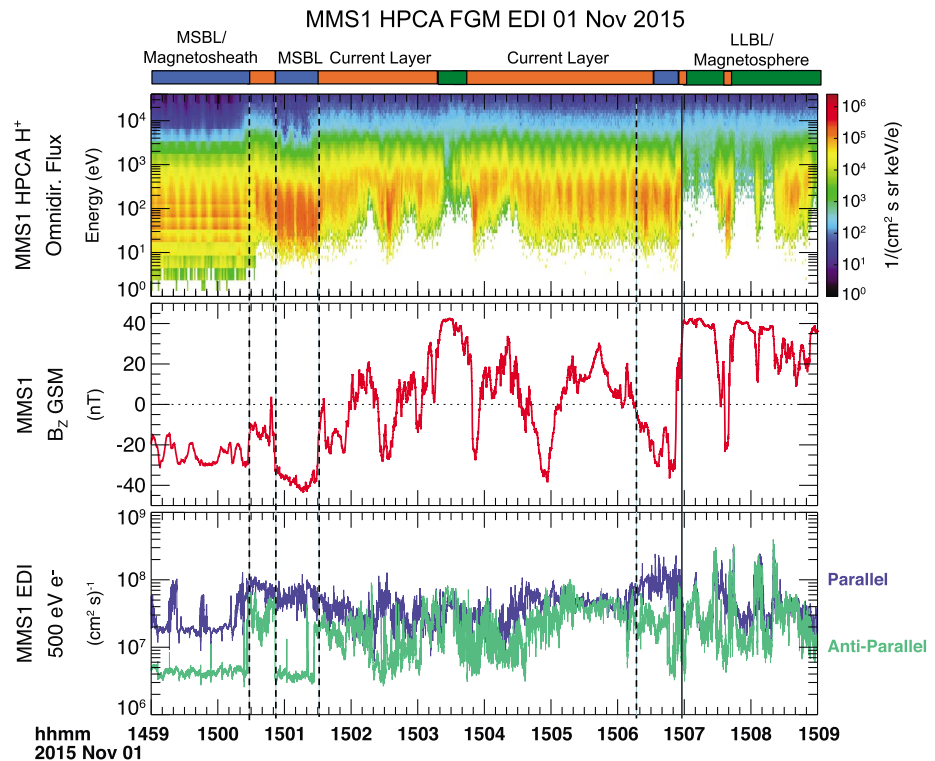
Figure 6. (top to bottom) Proton omnidirectional fluxes from MMS4, the B_z component of the magnetic field from MMS1, 800 eV electron fluxes parallel and antiparallel to the magnetic field from MMS1, the B_z component of the magnetic field from MMS4, and the 800 eV electron fluxes parallel and antiparallel to the magnetic field from MMS4. MMS4 is about 40 km closer to the Earth than MMS1, and the two spacecraft are nearly aligned along the normal direction to the magnetopause current layer. From 07:49:08 UT to 07:51:00 UT, MMS4 observes enhanced bidirectional streaming electron fluxes either longer or more often than MMS1 observes them. A notable exception is the two bursts of enhanced electron fluxes near 07:50 UT observed by MMS1, while MMS4 observes only one burst. This two-spacecraft comparison of the electron fluxes is largely consistent with a quasi-stationary reconnection X-line geometry shown in Figure 4 that sweeps over the two spacecraft.

secondary X-line. This staggered reconnection produces the layered field line topology that is shown schematically in Figure 4.

Since MMS is a multispacecraft mission, this quasi-steady interpretation is testable. Figure 6 shows ion observations from MMS4 and magnetic field and electron observations from MMS1 and MMS4. The panels from top to bottom are the MMS4 H^+ energy-time spectrogram, the B_z component of the magnetic field from MMS1, the electron fluxes at 800 eV parallel and antiparallel to the magnetic field from MMS1, the B_z component from MMS4, and the electron fluxes from MMS4. Two minutes of data are shown in Figure 6 from the final exit of the current layer at 07:49:08 UT to 07:59:00 UT.

The MMS spacecraft were approximately in a tetrahedron formation, except that MMS4 was about 80 km from MMS1 in the normal direction, with MMS4 closer to Earth than MMS1 [*Chen et al.*, 2016]. Provided the normal direction to the magnetopause is approximately constant, MMS4 should cross the magnetopause later than MMS1, and it should remain inside of the MSBL (and observe heated electrons) longer than MMS1.

Figure 6 shows that these expectations are more or less met; however, the differences are very subtle. Both spacecraft remain in the current layer until 07:49:08 UT when MMS4 appears to exit before MMS1. From

Figure 7. Observations from the magnetopause crossing associated with the event on 1 November 2015. (top to bottom) Proton omnidirectional flux, the B_z component of the magnetic field, and the 500 eV electron flux parallel and antiparallel to the magnetic field. In the three MSBL intervals, from 14:59 UT to 15:00:30 UT, from 15:00:50 UT to 15:01:30 UT, and from 15:06:10 UT to 15:06:55 UT, the spacecraft observes enhanced fluxes at 500 eV predominantly parallel to the magnetic field. However, there are brief instances when the antiparallel fluxes are also enhanced. Like the observations in Figures 5 and 6, these enhanced fluxes are consistent with the spacecraft traversing an island structure between two reconnection lines as shown in the right-hand side of Figure 4.

07:49:08 UT to 07:49:40 UT, MMS4 generally remains in the MSBL longer than MMS1 as evidenced by the longer duration of bursts of unidirectional and bidirectional streaming electrons. One example of this longer residence in the MSBL for MMS4 compared to MMS1 is shown by the dashed line at 07:49:32 UT. Again, these observations are consistent with the structure in Figure 4 and the fact that MMS4 is closer to Earth along the magnetopause normal. The two-spacecraft observations in Figure 6 largely confirm the quasi-steady interpretation in Figure 4, but these observations also demonstrate that the spacecraft are so close together that the differences are subtle. To be sure, there are a few instances after 07:49:08 UT when MMS1 observes heated, streaming electrons while MMS4 does not. Most notable is the burst of streaming electrons at 07:50:02 UT (shown by the dashed line) observed by MMS1 and not by MMS4. However, these instances appear to be more the exception than the rule. These instances may indicate a more complicated, three-dimensional geometry than the simplified two-dimensional geometry shown in Figure 4 [e.g., *Galeev et al.*, 1986].

Figure 7 shows another magnetopause crossing near the event on 1 November 2015. The format is the same as in Figure 5 except that the Electron Drift Instrument (EDI) [*Torbert et al.*, 2016] provided the electron fluxes. EDI makes active measurements of the electric field using a pair of electron beam and detector units. However, the detector units also operate in a passive mode to measure ambient electrons at a single energy over a very wide range of angles with very high time resolution [*Torbert et al.*, 2016]. In fast survey mode, the fluxes parallel and antiparallel to the magnetic field at 500 eV are transmitted to the ground with approximately 30 ms resolution.

MMS1 crossed the magnetopause from the magnetosheath to the magnetosphere over the 10 min shown. From 14:59 UT to 15:01:30 UT, the spacecraft was in the magnetosheath and MSBL, except for a short interval in the current layer from 15:00:25 UT to 15:00:50 UT, between the dashed lines. The next dashed line at

15:01:30 UT marks the rotation in the magnetic field that begins a relatively long current layer interval. The spacecraft exits this long current layer interval, returning briefly to the MSBL at about 15:05 UT and after the dashed line 15:06 UT. The final full crossing of the magnetopause occurred at 15:06:55 UT. In the magnetosheath proper, for example, centered on 15:00 UT, the electron fluxes parallel and antiparallel to the magnetic field are not equal. There are a variety of reasons for this imbalance, including bulk flow of the magnetosheath electrons along the field and heat flux from the solar wind. However, the transition from the magnetosheath proper to the MSBL and current layer is clearly evident in the dramatic increase in electron fluxes parallel and antiparallel to the field.

The heated, streaming electrons parallel to the magnetic field in the MSBL, for example, centered at 14:59:20 UT and 14:59:50 UT, indicate that the crossing on 1 November 2015 occurred southward of a primary X-line. Unlike the 19 September 2015 crossing, this primary X-line was probably centered on a nearly antiparallel magnetic shear region at the magnetopause. The IMF was strongly southward, and the magnetic shear conditions at the magnetopause and the spacecraft location were similar to those on 12 November 2015 shown in the bottom right-hand panel of Figure 2.

Although there are several intervals of heated electrons streaming parallel to the magnetic field, there are also a few, brief intervals where there are bidirectional streaming electrons. For example, there is a short burst and a longer interval of bidirectional streaming electrons just before the beginning of the long current layer interval at the dashed line at 15:01:30 UT and in the short MSBL interval at about 15:05 UT. Thus, the magnetic field structure is similar to the schematic in the right-hand panel of Figure 4, with the spacecraft remaining southward of the primary X-line. The four spacecraft were separated by only about 10 km during the 1 November 2015 crossing. Therefore, it is more difficult to identify differences in multispacecraft observations as was done in Figure 6 for the 19 September 2015 event.

Electron observations from the other 10 X-line events were used to determine if there was evidence of magnetic islands during these events. For two of the events (6 December 2015 and 14 December 2015), the time spent in the MSBL was very short and it was difficult to determine if bidirectional heated, streaming electrons were observed. Without a full transition from the MSBL into the magnetosheath proper, it is difficult to determine the qualitative level of electron heating in either directions along the magnetic field in the reconnection exhaust. However, for the remaining seven events, there was evidence of magnetic islands present at the magnetopause. Thus, for the majority of the EDR events, there is evidence of multiple, active X-lines at the magnetopause. Whether MMS made observations in the vicinity of the primary or secondary X-line is not known, and it is not clear how important knowing this is for understanding the fundamental microphysics of reconnection.

8. Discussion and Conclusions

To date, 12 X-line region events have been identified in the MMS data from mission phase 1a, the first pass of the dayside magnetopause. The reconnection electron diffusion region at the magnetopause is very small and the MMS spacecraft reside in or near the region for at most a few seconds. Basic questions about reconnection require observations in or near this region and the high time resolution measurements from the MMS spacecraft have resulted in several discoveries about the nature of reconnection at the magnetopause (see the references listed in Table 1).

Since reconnection is a fundamental process, it is important that it is investigated over the widest possible range of conditions. In particular, it is important to determine if the identification process for electron-scale physics in or near the EDR is robust and events are identified over a wide range of external conditions. Here the 12 X-line events were considered as a group and the external and internal conditions were investigated to determine if they span the range of conditions possible at the dayside magnetopause.

Figure 1 shows that the magnetopause crossings near the 12 X-line events occurred over a wide range of local times. With the 12 R_E apogee of the MMS orbit during phase 1a, magnetopause crossings occurred over the full local time range from 06:00 to 18:00 LT. However, the crossings were much more numerous between 07:00 and 17:00 LT, and the 12 events span this range. Furthermore, Figure 1 shows that the crossings occur over a wide range of radial distances from the Earth. Events closer (further) from the Earth than the nominal location occur because the dynamic pressure is greater than (or less than) nominal. In fact, the 12 events span

87% of the range of dynamic pressures that occurred during phase 1a. The X-line events that occurred during lower than nominal dynamic pressures are particularly important because they demonstrate that these reconnection regions are identifiable in the MMS data even when the magnetosheath density is relatively low. Thus, the identification of these events is not limited to extreme solar wind conditions.

All but one event occurred at the high magnetic shear magnetopause, when the IMF was southward. Figure 3 shows that 11 events had magnetic shear angles greater than 120°. The majority of the events (seven events total) occurred when the IMF B_y was dominant. The upper right-hand panel of Figure 2 shows that the Maximum Magnetic Shear Model does a reasonably good job of predicting the MMS spacecraft location near a component X-line under these IMF conditions. Observations of electron streaming in Figures 5 and 6 confirmed the spacecraft location relative to this primary X-line. In some other IMF orientations, namely, when IMF B_x is dominant, the Maximum Magnetic Shear Model is not as accurate in predicting the location of the X-line or the type of reconnection. However, the limitations to the model are known and there is current research to try to improve the model for these conditions. Two IMF orientations that have no event associated with them are when $\pm B_y$ or $\pm B_x$ is dominant when the IMF is northward. Under these conditions (not covered by the Maximum Magnetic Shear Model), it might be that the reconnection lines are confined to high latitudes [*Fuselier et al.*, 2014], in which case the MMS orbit at low latitudes will never be in the vicinity of a reconnection X-line.

Low plasma beta conditions in the magnetosheath were originally thought to be conducive to magnetic reconnection at the magnetopause [e.g., *Paschmann et al.*, 1986]. However, later it was suggested that the change in plasma beta across the magnetopause is a more important parameter for asymmetric reconnection with a guide field [*Swisdak et al.*, 2003]. Figure 3 shows that when the change in plasma beta across the magnetopause and the magnetic shear angles at the reconnection site are taken into account, the 12 X-line events all fall within the region where reconnection is possible. The magnetic shear angles at the magnetopause range from about 120° to close to 180° for the 11 events when the IMF was southward. The minimum magnetic shear in the subsolar region for IMF southward conditions is approximately 90° [*Vines et al.*, 2015]. Thus, these events range over almost the largest possible magnetic shear angles and, by definition, have almost the widest range of guide field values possible.

The single event with a magnetic shear angle of 28° occurred for reconnection in Kelvin-Helmholtz vortices during northward IMF conditions on the flank of the magnetopause [*Eriksson et al.*, 2016]. Reconnection is possible only between the magnetosheath and an existing boundary layer. The change in plasma beta from the magnetosheath to the magnetosphere was large enough that the event would have fallen in the "reconnection suppressed" region in Figure 2, had there been reconnecting plasma directly between these two regions. Since KH waves tend to develop preferentially during northward IMF, especially when the $+B_z$ component is dominant and during periods of sustained large solar wind speed and density [e.g., *Kavosi and Raeder*, 2015; *Allen et al.*, 2016], MMS crossings of the dawn and dusk magnetopause during the later phases of the mission could result in the identification of more X-line events when the magnetic shear is small.

Tables 2 and 3 show that the 12 events occur under highly asymmetric conditions. Most often, the asymmetry comes from the change in plasma density between the magnetosheath and the magnetosphere. Table 2 shows that the magnetosheath magnetic field is at most a factor of 2 less than the magnetospheric field, and the two fields are equal in three events. However, there is little influence from magnetospheric ions on the reconnection rate and, by default, it is the change in plasma density across the magnetopause that contributes the most to the asymmetry.

Table 3 shows that the X-line events all occurred when there was at least a small flow shear across the reconnection X-line (i.e., in the L direction) at the magnetopause. However, these flow shears were typically less than the magnetosheath Alfvén velocity (also using the L component of the magnetic field). For three events, the ratio of the flow velocity to the Alfvén velocity was between 1 and 2. Thus, according to *Cowley and Owen* [1989], reconnection is possible for all events, but the X-lines for the three events with velocity ratios greater than one must convect along the magnetopause such that this velocity ratio is less than one in the moving frame. One of these events is the 19 September 2015 event, with $V_L/V_{AL} = 1.22$. The streaming direction of the heated electrons in the MSBL in Figures 5 and 6 (either unidirectional parallel to B or bidirectional) indicates that there is always a reconnection line above or poleward of the spacecraft when it is in the MSBL. Thus,

these observations are interpreted here to indicate a stationary X-line above the spacecraft. The uncertainty in the V_L/V_{AL} ratio is of the order of 10% to 20%, suggesting that the flow is only marginally super-Alfvénic. Table 3 shows that when the hybrid Alfvén velocity is used, the velocity ratio is very close to one and may be marginally sub-Alfvénic. However, there is no current theory suggesting that the hybrid Alfvén velocity is the more appropriate characteristic speed for reconnection at the magnetopause.

At least one theoretical study of isolated, antiparallel X-lines suggests that they move with the magnetosheath flow regardless of the magnitude of the flow [*Doss et al.*, 2015]. However, the majority of the events in Table 3 are associated with multiple X-lines, and it is not clear if isolated X-lines exist at the magnetopause. It may be that the range of flow velocities in Table 3 represents the entire range possible for quasi-stationary reconnection at the magnetopause. However, it may be that when there is a large magnetosheath flow, the region in and around the electron diffusion region is modified or the region may be moving too fast so that it is not readily identified. Distinguishing among these possibilities requires more observations further on the flanks of the magnetopause where the magnetosheath flow velocities are high.

Finally, electron measurements were used to investigate the stability of the reconnection X-line location and the presence of other X-lines in the vicinity of the events. Electron observations in the MSBL, such as those in Figures 5–7, indicate whether the spacecraft are north or south of a single X-line or between two X-lines. This evidence does not provide any information on the distance to the X-line or lines or the size of the magnetic islands or flux ropes.

For the magnetopause crossing on 19 September 2015 (Figures 5 and 6), the spacecraft were southward of a primary X-line and were often between a primary and a secondary X-line. A quasi-steady interpretation of these observations has reconnection occurring first at the primary X-line that is always north of the spacecraft and then later at a second X-line that is located south of the spacecraft. The location of the spacecraft relative to the primary reconnection X-line and the component (guide field) nature of the reconnection are consistent with the predictions from the Maximum Magnetic Shear Model reconnection X-line location (see Figure 2). A similar conclusion is obtained from the observations in Figure 7 from the magnetopause crossing on 1 November 2015. Evidence for magnetic islands was also present in magnetopause crossings near eight events and, for the remaining two events (6 December 2015 and 14 December 2015), the evidence was ambiguous because there was not sufficient time in the MSBL near the X-line events.

The widespread evidence for magnetic islands is consistent with the results of a recent survey of magnetic islands at the magnetopause near reconnection X-lines [*Vines et al.*, 2017]. This survey found magnetic islands at 80% of the magnetopause crossings, independent of whether the X-line had a large guide field or not.

In conclusion, the large-scale conditions in the magnetosheath and magnetosphere represent nearly the widest range possible for the 12 events observed during phase 1a of the MMS mission. There appears to be no sample biases toward extreme ends of this range (for example, the magnetic shear angles and dynamic pressures span almost the entire possible range and are not limited to high magnetic shear conditions or high dynamic pressure conditions). There are some external conditions that are not covered, notably when magnetospheric ions could have played a more important role and when reconnection is more symmetric. These conditions may be rare enough that the 4500 full and partial magnetopause crossings in phase 1a may not be sufficient to cover all external conditions or it may be that reconnection is truly suppressed in the presence of high densities of magnetospheric ions and no observations in or near an EDR are possible. The importance of multi-ion populations in symmetric reconnection may require the measurements in the magnetotail from the later phases of the MMS mission.

References

Allen, R. C., S. A. Livi, S. K. Vines, and J. Goldstein (2016), Magnetic latitude dependence of oxygen charge states in the global magnetosphere: Insights into solar wind-originating ion injection, *J. Geophys. Res. Space Physics*, 121, 9888–9912, doi:10.1002/2016JA022925.

Beidler, M. T. and P. A. Cassak (2011), Model for incomplete reconnection in sawtooth crashes. *Phys. Rev. Lett.*, 107, 255002.

Birn, J., J. E. Borovsky, and M. Hesse, (2008), Properties of asymmetric magnetic reconnection, *Phys. Plasmas*, 15, 032101.

Borovsky, J. E., and M. H. Denton (2006), Effect of plasmaspheric drainage plumes on solar wind/magnetosphere coupling, *Geophys. Res. Lett.*, 33, L20101, doi:10.1029/2006GL026519.

Borovsky, J. E., M. H. Denton, R. E. Denton, V. K. Jordanova, and J. Krall (2013), Estimating the effects of ionospheric plasma on solar wind/magnetosphere coupling via mass loading of dayside reconnection: Ion-plasma-sheet oxygen, plasmaspheric drainage plumes, and the plasma cloak, *J. Geophys. Res. Space Physics*, 118, 5695, doi:10.1002/jgra.50527.

Burch, J. L., T. E. Moore, R. B. Torbert, B. L. Giles (2016a) Magnetospheric multiscale overview and science objectives, *Space Sci. Rev.*, *199*(1–4), 5–21, doi:10.1007/s11214-015-0164-9.

Burch, J. L., et al. (2016b), Electron-scale measurements of magnetic reconnection in space, *Science*, *352*, aaf2939, doi:10.1126/science.aaf2939.

Burch, J. L., and T. D. Phan (2016), Magnetic reconnection at the dayside magnetopause: Advances with MMS, *Geophys. Res. Lett.*, *43*, 8327–8338, doi:10.1002/2016GL069787.

Cassak, P. A., and M. A. Shay (2007), Scaling of asymmetric magnetic reconnection: General theory and collisional simulations, *Phys. Plasmas*, *14*, 102114, doi:10.1063/1.2795630.

Cassak, P. A., and S. A. Fuselier (2016), Reconnection at Earth's dayside magnetopause, in *Magnetic Reconnection, Astrophys. Space Sci. Lib.*, vol. 427, edited by W. Gonzalez and E. Parker, pp. 213–276, Springer, Switzerland, doi:10.1007/978-3-319-26432-5.

Chappell, C. R., M. M. Huddleston, T. E. Moore, B. L. Giles, and D. C. Delcourt (2008), Observations of the warm plasma cloak and an explanation of its formation in the magnetosphere, *J. Geophys. Res.*, *113*, A09206, doi:10.1029/2007JA012945.

Chen, L.-J., et al. (2016), Electron energization and mixing observed by MMS in the vicinity of an electron diffusion region during magnetopause reconnection, *Geophys. Res. Lett.*, *43*, 6036–6043, doi:10.1002/2016GL069215.

Cowley, S. W. H., and C. J. Owen (1989), A simple illustrative model of open flux tube motion over the dayside magnetopause, *Planet. Space Sci.*, *37*, 1461.

Crooker, N. U. (1979), Dayside merging and cusp geometry, *J. Geophys. Res.*, *84*, 951–959, doi:10.1029/JA084iA03p00951.

DiBraccio, G. A., J. A. Slavin, S. A. Boardsen, B. J. Anderson, H. Korth, T. H. Zurbuchen, J. M. Raines, D. N. Baker, R. L. McNutt Jr., and S. C. Solomon (2013), MESSENGER observations of magnetopause structure and dynamics at Mercury, *J. Geophys. Res. Space Physics*, *118*, 997–1008, doi:10.1002/jgra.50123.

Doss, C. E., C. M. Komar, P. A. Cassak, F. D. Wilder, S. Eriksson, and J. F. Drake, (2015), Asymmetric magnetic reconnection with a flow shear and applications to the magnetopause, *J. Geophys. Res. Space Physics*, *120*, 7748–7763, doi:10.1002/2015JA021489.

Drake, J. F., M. Swisdak, H. Che, and M. A. Shay (2006a), Electron acceleration from contracting magnetic islands during reconnection, *Nature*, *443*, 553–556, doi:10.1038/nature0511.6

Drake, J. F., M. Swisdak, K. M. Schoeffler, B. N. Rogers, and S. Kobayashi (2006b), Formation of secondary islands during magnetic reconnection, *Geophys. Res. Lett.*, *33*, L13105, doi:10.1029/2006GL025957.

Dunlop, M. W., et al. (2011), Magnetopause reconnection across wide local time, *Ann. Geophys.*, *29*, 1683.

Eriksson, S., et al. (2016), Magnetospheric multiscale observations of magnetic reconnection associated with Kelvin-Helmholtz waves, *Geophys. Res. Lett.*, *43*, 5606–5615, doi:10.1002/2016GL068783.

Fuselier, S. A., and W. S. Lewis (2011), Properties of near-Earth magnetic reconnection from in-situ observations, *Space Sci. Rev.*, *160*, 95–121, doi 10.1007/s11214-011-9820-x.

Fuselier, S. A., B. J. Anderson, and T. G. Onsager (1995), Particle signatures of magnetic topology at the magnetopause: AMPTE/CCE observations, *J. Geophys. Res.*, *100*, 11,805–11,822.

Fuselier, S. A., S. M. Petrinec, and K. J. Trattner (2000), Stability of the high-latitude reconnection site for steady northward IMF, *Geophys. Res. Lett.*, *27*, 473–476.

Fuselier, S. A., K. J. Trattner, and S. M. Petrinec (2011), Anti-parallel and component reconnection at the dayside magnetopause, *J. Geophys. Res.*, *116*, A10227, doi:10.1029/2011JA016888.

Fuselier, S. A., K. J. Trattner, S. M. Petrinec, and B. Lavraud (2012), Dayside magnetic topology at the Earth's magnetopause for northward IMF, *J. Geophys. Res.*, *117*, A08235, doi:10.1029/2012JA017852.

Fuselier, S. A., R. Frahm, W. S. Lewis, A. Masters, J. Mukherjee, S. M. Petrinec, and I. J. Sillanpaa (2014), The location of magnetic reconnection at Saturn's magnetopause—A comparison with Earth, *J. Geophys. Res. Space Physics*, *119*, 2563–2578, doi:10.1002/2013JA019684.

Fuselier, S. A., W. S. Lewis, C. Schiff, R. Ergun, J. L. Burch, S. M. Petrinec, and K. J. Trattner (2016a), Magnetospheric multiscale science mission profile and operations, *Space Sci. Rev.*, *199*(1–4), 77–103.

Fuselier, S. A., et al. (2016b), Magnetospheric ion influence on magnetic reconnection at the duskside magnetopause, *Geophys. Res. Lett.*, *43*, 1435–1442, doi:10.1002/2015GL067358.

Galeev, A. A., M. M. Kuznetsova, L. M. Zeleny (1986), Magnetopause stability threshold for patchy reconnection, *Space Sci. Rev.*, *44*, 1–41, doi:10.1007/BF00227227.

Gomez, R. G., et al. (2016), Stable reconnection at the dusk flank magnetopause, *Geophys. Res. Lett.*, *43*, 9374–9382, doi:10.1002/2016GL069692.

Gonzalez, W. D., and F. S. Mozer (1974), A quantitative model for the potential resulting from reconnection with an arbitrary interplanetary magnetic field, *J. Geophys. Res.*, *79*, 4186–4194, doi:10.1029/JA079i028p04186.

Gosling, J. T., M. F. Thomsen, S. J. Bame, T. G. Onsager, and C. T. Russell (1990), The electron edge of the low latitude boundary layer during accelerated flow events, *Geophys. Res. Lett.*, *17*, 1933–1836.

Gosling, J. M., M. F. Thomsen, S. J. Bame, R. C. Elphic, and C. T. Russell (1991), Observations of reconnection of interplanetary and lobe magnetic field lines at the high-latitude magnetopause, *J. Geophys. Res.*, *96*, 14,097.

Graham, D. B., et al. (2016), Electron currents and heating in the ion diffusion region of asymmetric reconnection, *Geophys. Res. Lett.*, *43*, 4691–4700, doi:10.1002/2016GL068613.

Hasegawa, H., et al. (2010), Evidence for a flux transfer event generated by multiple X-line reconnection at the magnetopause, *Geophys. Res. Lett.*, *37*, L16101, doi:10.1029/2010GL044219.

Hesse, M. (2006), Dissipation in magnetic reconnection with a guide magnetic field, *Phys. Plasmas*, *13*, 1220107.

Kavosi, S., and J. Raeder (2015), Ubiquity of Kelvin-Helmholtz waves at Earth's magnetopause, *Nat. Commun.*, *6*, 7019 doi:10.1038/ncomms8019.

Khotyaintsev, Y. V., et al. (2016), Electron jet of asymmetric reconnection, *Geophys. Res. Lett.*, *43*, 5571–5580, doi:10.1002/2016GL069064.

Komar, C. M., R. L. Fermo, and P. A. Cassak (2015), Comparative analysis of dayside magnetic reconnection models in global magnetosphere simulations, *J. Geophys. Res. Space Physics*, *120*, 276–294, doi:10.1002/2014JA020587.

Lavraud, B., M. F. Thomsen, B. Lefebvre, S. J. Schwartz, K. Seki, T. D. Phan, Y. L. Wang, A. Fazakerley, H. Rxeme, and A. Balogh (2006), Evidence for newly closed magnetosheath field lines at the dayside magnetopause under northward IMF, *J. Geophys. Res.*, *111*, A05211, doi:10.1029/2005JA011266.

Lavraud, B., A. Fedorov, E. Budnik, M. F. Thomsen, A. Grigoriev, P. J. Cargill, M. W. Dunlop, H. Rème, I. Dandouras, and A. Balogh (2005a), High-altitude cusp flows dependence on IMF orientation: A three-year Cluster statistical study, *J. Geophys. Res.*, *110*, A02209, doi:10.1029/2004JA010804.

Lavraud, B., M. F. Thomsen, M. G. G. T. Taylor, Y. L. Wang, T. D. Phan, S. J. Schwartz, R. C. Elphic, A. Fazakerley, H. R'eme, and A. Balogh (2005b), Characteristics of the magnetosheath electron boundary layer under northward interplanetary magnetic field: Implications for high-latitude reconnection, *J. Geophys. Res.*, *110*, A06209, doi:10.1029/2004JA010808.

Lavraud, B., et al. (2016), Currents and associated electron scattering and bouncing near the diffusion region at Earth's magnetopause, *Geophys. Res. Lett.*, *43*, 3042–3050, doi:10.1002/2016GL068359.

Mozer, F. S., S. D. Bale, and T. D. Phan (2002), Observations of ion and electron diffusion regions at a sub-solar magnetopause reconnection event. *Phys. Rev. Lett.*, *89*, 015002.

Norgren, C., et al. (2016), Finite gyroradius effects in the electron outflow of asymmetric magnetic reconnection, *Geophys. Res. Lett.*, *43*, 6724–6733, doi:10.1002/2016GL069205.

Øieroset, M., T. D. Phan, M. Fujimoto, R. P. Lin and R. P. Lepping (2001), In situ detection of collisionless reconnection in the Earth's magnetotail, *Nature*, *412*, 414.

Øieroset, M., et al. (2011), Direct evidence for a three-dimensional magnetic flux rope flanked by two active magnetic reconnection X lines at Earth's magnetopause, *Phys. Rev. Lett.*, *107*, 165007.

Øieroset, M., D. Sundkvist, C. C. Chaston, T. D. Phan, F. S. Mozer, J. P. McFadden, V. Angelopoulos, L. Andersson, and J. P. Eastwood (2014), Observations of plasma waves in the colliding jet region of a magnetic flux rope flanked by two active X lines at the subsolar magnetopause, *J. Geophys. Res. Space Physics*, *119*, 6256–6272, doi:10.1002/2014JA020124.

Øieroset, M., T. D. Phan, J. T. Gosling, M. Fujimoto, and V. Angelopoulos (2015), Electron and ion edges and the associated magnetic topology of the reconnecting magnetopause, *J. Geophys. Res. Space Physics*, *120*, 9294–9306, doi:10.1002/2015JA021580.

Øieroset, M., et al. (2016), MMS observations of large guide field 1 symmetric reconnection between colliding reconnection jets at the center of a magnetic flux rope at the magnetopause, *Geophys. Res. Lett.*, *43*, 5536–5544, doi:10.1002/2016GL069166.

Olsen, R. C., S. D. Shawhan, D. L. Gallagher, J. L. Green, C. R. Chappell, and R. R. Anderson (1987), Plasma observations at the Earth's magnetic equator, *J. Geophys. Res.*, *92*, 2385–2407, doi:10.1029/JA092iA03p02385.

Paschmann, G., et al. (1986), The magnetopause for large magnetic shear: AMPTE/IRM observations, *J. Geophys. Res.*, *91*, 11,099–11,115.

Paschmann, G., M. Øieroset, and T. D. Phan (2013), Observations of reconnection in space, *Space Sci. Rev.*, *178*, 385–417, doi 10.1007/s11214-012-9957-2.

Petrinec, S. M., et al. (2011), Neutral atom imaging of the magnetospheric cusp, *J. Geophys. Res.*, *116*, A07203, doi:10.1029/2010JA016357.

Phan T. D., et al. (2007), Evidence for an elongated (>60 ion skin depths) electron diffusion region during fast magnetic reconnection, *Phys. Rev. Lett.*, *99*(25), 255002, doi:10.1103/PhysRevLett.99255002.

Phan, T., et al. (2003), Simultaneous Cluster and IMAGE observations of cusp reconnection and auroral proton spot for northward IMF, *Geophys. Res. Lett.*, *30*(10), 1509, doi:10.1029/2003GL016885.

Phan, T. D., et al. (2010), The dependence of magnetic reconnection on plasma B and magnetic shear: Evidence from solar wind observations, *Astrophys. J. Lett.*, *719*, L199, doi:10.1088/2041-8205/719/2/L199.

Phan, T. D., G. Paschmann, J. T. Gosling, M. Oieroset, M. Fujimoto, J. F. Drake, and V. Angelopoulos (2013), The dependence of magnetic reconnection on plasma β and magnetic shear: Evidence from magnetopause observations, *Geophys. Res. Lett.*, *40*, 11–16, doi:10.1029/2012GL054528.

Phan, T. D., et al. (2016), MMS observations of electron-scale filamentary currents in the reconnection exhaust and near the X line, *Geophys. Res. Lett.*, *43*, 6060–6069, doi:10.1002/2016GL069212.

Pollock, C., et al. (2016), Fast plasma investigation for magnetospheric multiscale, *Space Sci. Rev.*, *199*, 331–406, doi: 10.1007/s11214-016-0245-4.

Roelof, E. C., and D. G. Sibeck (1993), Magnetopause shape as a bivariate function of interplanetary field B_z and solar wind dynamic pressure, *J. Geophys. Res.*, *98*, 21,421.

Russell, C. T., et al. (2016), The magnetospheric multiscale magnetometers, *Space Sci. Rev.*, *199*, 189–256, doi:10.1007/s11214-014-0057-3.

Sonnerup, B. U. Ö. (1974), Magnetopause reconnection rate, *J. Geophys. Res.*, *79*, 1546–1549, doi:10.1029/JA079i010p01546.

Shay, M. A., J. F. Drake, R. E. Denton, and D. Biskamp (1998), Structure of the dissipation region during collisionless magnetic reconnection, *J. Geophys. Res.*, *103*, 9165–9176.

Swisdak, M., et al. (2003), Diamagnetic suppression of component magnetic reconnection at the magnetopause, *J. Geophys. Res.*, *108*(A5), 1218, doi:10.1029/2002JA009726.

Swisdak, M., M. Opher, J. F. Drake, and F. Alouani Bibi (2010), The vector direction of the interstellar magnetic field outside the heliosphere, *Astrophys. J.*, *710*, 1769.

Torbert, R. B., et al. (2016), The electron drift instrument for MMS, *Space Sci. Rev.*, *199*, 283–305 doi:10.1007/s11214-015-0182-7.

Trattner, K. J., J. S. Mulcock, S. M. Petrinec, and S. A. Fuselier (2007a), Location of the reconnection line at the magnetopause during southward IMF conditions, *Geophys. Res. Lett.*, *34*, L03108, doi:10.1029/2006GL028397.

Trattner, K. J., J. S. Mulcock, S. M. Petrinec, and S. A. Fuselier (2007b), Probing the boundary between anti-parallel and component reconnection during southward interplanetary magnetic field conditions, *J. Geophys. Res.*, *112*, A08210, doi:10.1029/2007JA012270.

Trattner, K. J., S. M. Petrinec, S. A. Fuselier, N. Omidi, and D. G. Sibeck (2012), Evidence of multiple reconnection lines at the magnetopause from cusp observations, *J. Geophys. Res.*, *117*, A01213, doi:10.1029/2011JA017080.

Trattner, K. J., S. Thresher, L. Trenchi, S. A. Fuselier, S. M. Petrinec, W. K. Peterson, and M. F. Marcucci (2017), On the occurrence of magnetic reconnection equatorward of the cusps at the Earth's magnetopause during northward IMF conditions, *J. Geophys. Res. Space Physics*, *122*, 605–617, doi:10.1002/2016JA023398.

Vernisse, Y., et al. (2016), Signatures of complex magnetic topologies from multiple reconnection sites induced by Kelvin-Helmholtz instability, *J. Geophys. Res. Space Physics*, *121*, 9926–9939, doi:10.1002/2016JA023051.

Vines, S. K., S. A. Fuselier, K. J. Trattner, S. M. Petrinec, and J. F. Drake (2015), Ion acceleration dependence on magnetic shear angle in dayside magnetopause reconnection, *J. Geophys. Res. Space Physics*, *120*, 7255–7269, doi:10.1002/2015JA021464.

Vines, S. K., S. A. Fuselier, S. M. Petrinec, K. J. Trattner, and R. C. Allen (2017), Occurrence frequency and location of magnetic islands at the dayside magnetopause, *J. Geophys. Res. Space Physics*, *122*, 4138–4155, doi:10.1002/2016JA023524.

Walsh, B. M., D. G. Sibeck, Y. Nishimura, and V. Angelopoulos (2013), Statistical analysis of the plasmaspheric plume at the magnetopause, *J. Geophys. Res. Space Physics*, *118*, 4844–4851, doi:10.1002/jgra.50458.

Wang, S., L. M. Kistler, C. G. Mouikis, and S. M. Petrinec (2015), Dependence of the dayside magnetopause reconnection rate on local conditions, *J. Geophys. Res. Space Physics*, *120*, 6376–6408, doi:10.1002/2015JA021524.

Wilder, F. D., S. Eriksson, K. J. Trattner, P. A. Cassak, S. A. Fuselier, and B. Lybekk (2014), Observation of a retreating x-line and magnetic islands poleward of the cusp during northward interplanetary magnetic field conditions, *J. Geophys. Res. Space Physics*, *119*, 9643–9657, doi:10.1002/2014JA020453.

Young, D. T., et al. (2016), Hot Plasma Composition Analyzer for the magnetospheric multiscale mission, *Space Sci. Rev.*, *199*(1–4), 407–470.